IEEE Access
Multidisciplinary ⋮ Rapid Review ⋮ Open Access Journal

Received 26 November 2023, accepted 10 December 2023, date of publication 13 December 2023,
date of current version 19 December 2023.

Digital Object Identifier 10.1109/ACCESS.2023.3342177

RESEARCH ARTICLE

Evolved Quasi-3D Analysis Method for Analysis Cost Reduction of Axial Flux Permanent Magnet Motor

JONG-MIN AHN[1], HAN-KYEOL YEO[2], JI-YEON KIM[3], DONG-HEE LEE[3], AND DONG-KUK LIM[1]

[1]Department of Electrical, Electronic and Computer Engineering, University of Ulsan, Nam-gu, Ulsan 44610, South Korea
[2]Division of Electrical and Electronic Engineering, The University of Suwon, Hwaseong-si 18323, South Korea
[3]Department of Advanced Electrification Engineering Design Team, Hyundai Motor Company, Hwaseong-si 18280, Republic of Korea

Corresponding author: Dong-Kuk Lim (ldk8745@ulsan.ac.kr)

This work was supported by the National Research Foundation of Korea (NRF) grant funded by the Korean Government (MSIT) under Grant 2022R1A2C2092905.

ABSTRACT This paper proposes an evolved quasi-3D analysis method (EQAM) that can extremely reduce analysis time by applying it to models where 3D analysis is essential. The conventional quasi-3D analysis is a method that can equalize a 3D analysis with multiple 2D analyses and is widely used for 3D models that take a long analysis time. However, the quasi-3D method still has the problem of taking a long time to interpret because it requires increasing the number of quasi segments to obtain accurate results. Therefore, this paper proposes a method of deriving a magnetic flux linkage, torque, voltage, torque-current phase angle curve (T-β curve) by interpreting only one step rather than all steps in multiple quasi segments. Compared to the 3D analysis, the EQAM reduced the T-β curve extraction time by 99.1% and reduced the capacity of the analysis file by 99.6%. In terms of analysis accuracy, the average torque error rate is 0.20% and the voltage error rate is 2.88% at the operating point. The validity of the proposed method was verified by confirming that the analysis time and file capacity reduction rate were significantly higher than the error rate. Therefore, EQAM is expected to be of great help to researchers facing time problems by being applied to various fields and studies that require 3D finite element analysis.

INDEX TERMS Electromagnetic analysis, finite element analysis, permanent magnet motors, quasi-3D, yokeless and segmented armature.

I. INTRODUCTION

The interest in eco-friendly urban air mobility (UAM) that can take off and land vertically is increasing due to extreme traffic congestion and environmental pollution caused by overcrowding in metropolises around the world [1], [2], [3], [4], [5], [6]. The global UAM market is expected to grow steadily at an annual average of 30.2% from 2022 to 2031 [7]. German private aircraft company Volocopter conducted a noise measurement test near Paris, France at the end of March 2020 by flying 50 to 70 meters in a two-seater air taxi with a real person [8]. Therefore, the commercialization of the UAM is not very far. In addition, unmanned aerial vehicles (UAV) for cargo transportation can be used for high-speed transportation of medium-sized cargo between cities that are difficult to operate with existing road and water infrastructure, and it is expected to lay the foundation for innovation in urban logistics services by increasing the accessibility of air transport. The market for UAV deliveries is expected to increase with a growth rate of approximately 20% in 2030 and the number of delivery UAVs is rising rapidly from 7 thousand in 2020 to assumed 125 thousand in 2035 [9], [10].

The high-power density and output power per unit weight are important for propulsion motors for vertical take-off and landing UAM. To meet these conditions, it is necessary to

The associate editor coordinating the review of this manuscript and approving it for publication was Zhuang Xu.

develop design technology of axial flux permanent magnet motor (AFPMM) with high power density at low speed among electric motor types and yokeless and segmented armature (YASA) that can maximize output power per unit weight among AFPMMs [11], [12], [13].

As shown in Fig.1, AFPMM is divided into single stator single rotor (SSSR), double stator single rotor (DSSR), single stator double rotor (SSDR), multi stator multi rotor (MSMR) types by the arrangement and number of stator and rotor [14], [15], [16], [17]. The YASA type has an SSDR structure by symmetrically arranging the rotor to remove excessive axial force, which is a problem that occurs in the SSSR type. The magnets can remove magnetically unnecessary stator yoke by placing opposite facing magnetic poles.

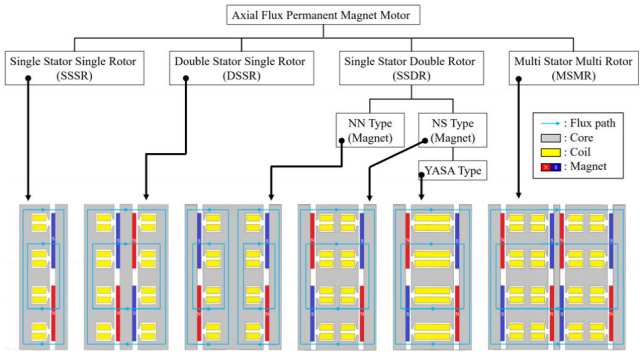

FIGURE 1. The type and magnetic flux path of the AFPMMs.

Due to these structural advantages, it is possible to reduce the motor size by increasing the space factor and reducing the stack length and increase efficiency by reducing iron loss and coil end winding. Therefore, the YASA model is suitable as a UAM propulsion motor that requires high power density and power per unit weight. However, the YASA model requires appropriate consideration such as axial force analysis and support structure. Because there is no yoke of the stator, the end of the motor may be bent by centrifugal force during high-speed rotation. In addition, there is a problem that it takes a long time to analysis since 3D analysis is essential structurally [18].

Many studies are in progress to solve this problem, and among them, Quasi-3D analysis is a method of equivalent analysis of 3D analysis to 2D analysis, and it is a method that can derive similar analysis results without 3D analysis [19], [20], [21], [22], [23]. However, conventional quasi-3d need to increase the number of quasi segments to obtain convergent results. In other words, there is still an analysis time problem since several 2D analyses are required. Therefore, in this paper, evolved quasi-3D analysis method (EQAM) is proposed that can derive torque, voltage, and torque-speed characteristic curves (T-N curve) by interpreting only one step rather than the entire step of several 2D analyses to interpret faster than the conventional quasi-3D.

Chapter 2 deals with the basic reference frame transformation required to analyze the characteristics of permanent magnet synchronous motor (PMSM), the load characteristic calculation formula for deriving the T-N curve, and the flow chart of the T-N curve. Chapter 3 consists of the specification and simulation results of the YASA model. Chapter 4 consists of the basic principles and verification of the quasi-3d method, Chapter 5 consists of the explanation and verification of 3D-1step analysis method, and Chapter 6 consists of the description and verification of EQAM.

II. REFERENCE FRAME TRANSFORMATION FOR CHARACTERISTIC ANALYSIS OF PMSM

A. REFERENCE FRAME TRANSFORMATION

The transformation of a, b, and c phase variables with a phase difference of 120°, which are used when dealing with three-phase alternating current motors, into variables on the d-q axis orthogonal coordinate system with a phase difference of 90° is called reference frame transformation. Generally, the vector control is used to simplify the control of the input current, the d axis is the magnetic flux axis of the permanent magnet that generates the rotor magnetic flux, and the q axis is the axis of the motor torque that must be generated by the stator magnetic field [24], [25], [26].

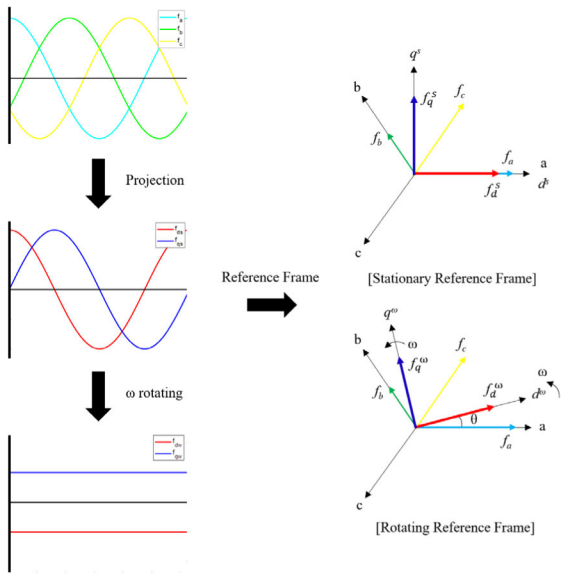

FIGURE 2. Reference frame transformation.

Left of the Fig. 2 shows the process of converting a three-phase variable in the a, b, and c coordinate system into a d^s -q^s axis variable in a stationary orthogonal coordinate system and converting them into the rotating coordinate system again. Right of the Fig. 2 represents coordinate transformation process in a coordinate system. It is expressed as follows by projecting the variables f_a, f_b, and f_c of the a, b, and c coordinate system into the d-q axis coordinate axis.

$$f_d^s = k\left[f_a\cos(0) + f_b\cos\left(-\frac{2}{3}\pi\right) + f_c\cos\left(-\frac{4}{3}\pi\right)\right] \quad (1)$$

$$f_q^s = k\left[-f_a\sin(0) - f_b\sin\left(-\frac{2}{3}\pi\right) - f_c\sin\left(-\frac{4}{3}\pi\right)\right] \quad (2)$$

The k is transformation coefficient and can adjust the size of the converted value. The variables in the a, b and c coordinate system need to be changed to the rotating d-q axis variable since the d-q axis can be rotated, and the equation for converting the three-phase variables in the a, b and c coordinate system into the d^s-q^s axis variable in the orthogonal coordinate system rotating at any angular velocity ω is as follow.

$$f_{dq}^{\omega} = T(\theta) f_{abc} \tag{3}$$

where $f_{dq} = [f_d\ f_q]$, $f_{abc} = [f_a f_b f_c]$, f is any motor variable and may be voltage, current, or magnetic flux linkage. The transformation matrix $T(\theta)$ and the rotation angle used in (3) are defined by the following equation.

$$T(\theta) = \frac{2}{3}\begin{bmatrix} \cos(\theta) & \cos(\theta - \frac{2}{3}\pi) & \cos(\theta - \frac{4}{3}\pi) \\ -\sin(\theta) & -\sin(\theta - \frac{2}{3}\pi) & -\sin(\theta - \frac{4}{3}\pi) \\ \frac{1}{2} & \frac{1}{2} & \frac{1}{2} \end{bmatrix} \tag{4}$$

$$\theta = \int \omega(t)dt + \theta(0) \tag{5}$$

The three-phase alternating current variables are expressed as direct current values in the d^{ω}-q^{ω} axis rotating coordinate system that rotates at the angular velocity of the alternating current, and the conversion from the static coordinate system to the rotating coordinate system is expressed as follow.

$$f_d^{\omega} = f_d^s \cos\theta + f_q^s \sin\theta \tag{6}$$

$$f_q^{\omega} = -f_d^s \sin\theta + f_q^s \cos\theta \tag{7}$$

B. CALCULATION OF THE LOAD CHARACTERISTICS

The load characteristics of the synchronous motor can be simply calculated using conversion to the d-q axis rotating coordinate system.

$$i_d = I_{max} \cos\beta \tag{8}$$

$$i_q = I_{max} \sin\beta \tag{9}$$

where I_{max} is magnitude of the current and β is phase of the current. The d-q-axis magnetic flux linkage is calculated using the previously defined transformation matrix $T(\theta)$. The equation is as follows (10)–(13), as shown at the bottom of the page, where L_{ls} is the stator leakage inductance, L_A is the average value of the magnetizing inductance, L_B is the variation value of the magnetizing inductance, and ϕ_f is the magnetic flux linkage by the permanent magnet. To simplify the (13), if $\theta = \theta_r$ is substituted and calculated, it is converted into a coordinate system that rotates with the angular velocity of the rotor.

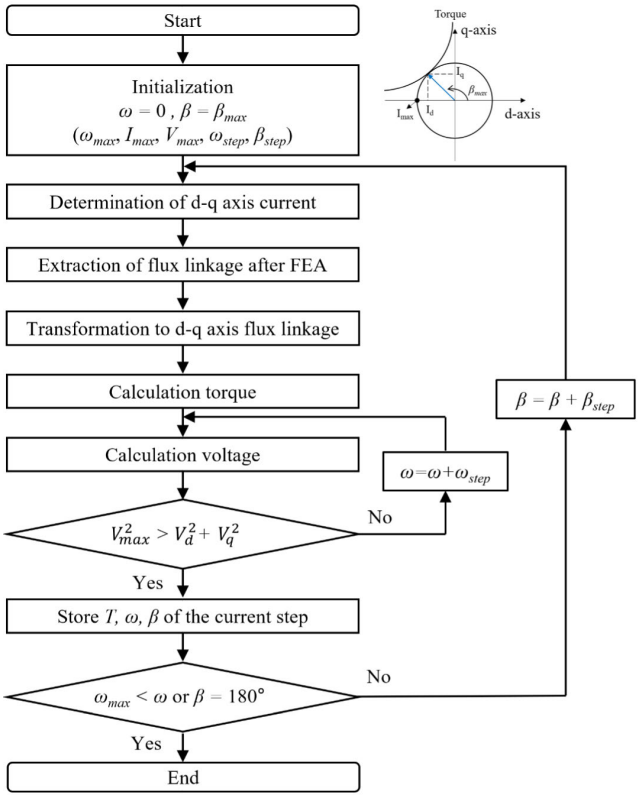

FIGURE 3. Flow chart of T-N Curve.

$$\lambda_{dq}^{r} = \begin{bmatrix} L_d & 0 \\ 0 & L_q \end{bmatrix} \begin{bmatrix} i_d^r \\ i_q^r \end{bmatrix} + \begin{bmatrix} \phi_f \\ 0 \end{bmatrix} \tag{14}$$

where $L_d = L_{ls}+3/2(L_A\text{-}L_B)$, $L_q = L_{ls}+3/2(L_A + L_B)$. The torque can be calculated using the calculated magnetic flux linkage and current as follows.

$$T_{cal} = \frac{3}{2}\frac{P}{2}\left(\lambda_d i_q - \lambda_q i_d\right) \tag{15}$$

$$\lambda_{abc} = L_s i_{abc} + L_f I_f \tag{10}$$

$$T(\theta)\lambda_{abc} = T(\theta)L_s i_{abc} + T(\theta)L_f I_f \tag{11}$$

$$\lambda_{dq}^{\omega} = T(\theta)L_s \left(T(\theta)^{-1}\right) i_{dq}^{\omega} + T(\theta)L_f I_f \tag{12}$$

$$\lambda_{dq}^{\omega} = \begin{bmatrix} L_{ls} + \frac{2}{3}L_A - \frac{2}{3}L_B\cos 2(\theta - \theta_r) & \frac{2}{3}L_B \sin 2(\theta - \theta_r) & 0 \\ \frac{2}{3}L_B \sin 2(\theta - \theta_r) & L_{ls} + \frac{2}{3}L_A + \frac{2}{3}L_B\cos 2(\theta - \theta_r) & 0 \\ 0 & 0 & L_{ls} \end{bmatrix} i_{dq}^{\omega} + \begin{bmatrix} \cos(\theta - \theta_r) \\ -\sin(\theta - \theta_r) \\ 0 \end{bmatrix} \phi_f \tag{13}$$

The voltage is calculated using the stator resistance and magnetic flux linkage as follows.

$$V_d = R_s i_d - \omega_r \lambda_q \tag{16}$$
$$V_q = R_s i_q + \omega_r \lambda_d \tag{17}$$
$$V_{cal} = \sqrt{V_d^2 + V_q^2} \tag{18}$$

In addition, the above equations are used to derive a T-N curve, which is an important characteristic curve in motor design. The flow chart for the T-N curve is shown in Fig. 3.

First, initial parameters such as maximum angular velocity, maximum current, voltage limit, current phase angle increment, and angular velocity increment are selected. The initial angular velocity is zero, and the current phase angle is selected as the current phase angle that generates the maximum torque at I_{max}.

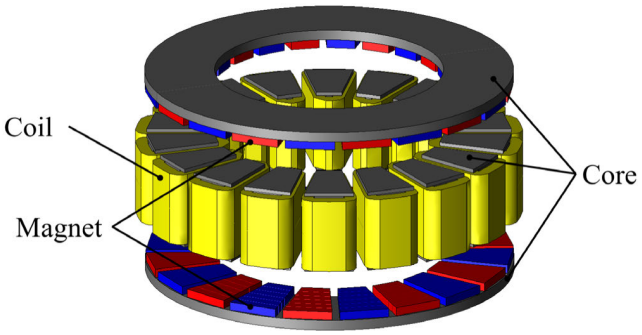

FIGURE 4. Shape of the YASA motor for UAM propulsion.

TABLE 1. Specifications of the YASA model.

Specification	Value	Unit
Pole / Slot	20 / 18	
Rotor inner / outer diameter	152 / 242	mm
Stator inner / outer diameter	152 / 242	mm
Air gap	1.3	mm
Stack length	86	mm
Magnet material	N42UH	
Core material	25PNX1250F	
Layer / Turns per layer	Double layer / 23	- / turns
Rated power	62.8	kW
Rated torque	150	Nm
Rated speed	4,000	RPM
Voltage limit	650	V_{dc}

The d-q axis current is calculated using the selected maximum current and current phase angle, and the finite element analysis (FEA) is performed by applying it to the corresponding model. The magnetic flux linkage of a, b, and c phases is extracted through FEA and converted into d-q axis magnetic flux linkage using a transformation matrix.

The torque and d-q axis voltage are calculated using magnetic flux linkage, and if the calculated voltage does not exceed the voltage limit, the angular velocity is increased by the specified angular velocity increment and the voltage is recalculated. If the voltage exceeds the voltage limit, the torque, current phase angle, and angular velocity are stored at the corresponding step.

If the stored angular velocity does not exceed the maximum angular velocity or the current phase angle does not exceed 180 degrees, increase by a predetermined current phase angle increment, and repeat the process from the d-q axis current calculation. If the angular velocity limit is exceeded or the current phase angle is 180 degrees, the algorithm is terminated.

III. 3D-FEA YASA MODEL FOR UAM PROPULSION

This chapter contains a description of the reference 3D model for comparison with other methods. The motor model for verification is a YASA type motor as shown in Fig. 4, and detailed design specifications are summarized in Table 1.

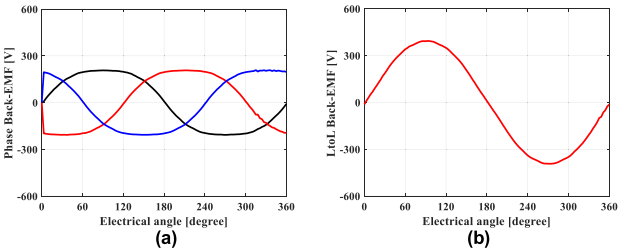

FIGURE 5. The noload results of the 3D-FEA (a) Phase Back-EMF (b) Line to Line Back-EMF.

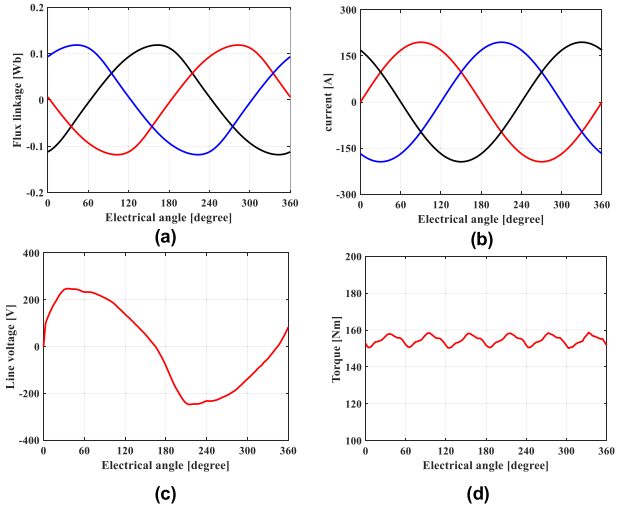

FIGURE 6. The load results of the 3D-FEA (a) magnetic flux linkage (b) current (c) line voltage (d) torque.

The results of the no-load analysis and load analysis for the YASA model are confirmed. The Fig. 5 shows the phase back-EMF and line to line back-EMF waveforms as a result of the no-load analysis. The Fig. 6 shows the magnetic flux linkage, input current, voltage, and torque waveforms as a result of the load analysis. The Fig. 7 shows torque-current phase angle curve (T-β curve) and the T-N curve. Table 2 summarizes the analysis results for the 3D-FEA YASA model.

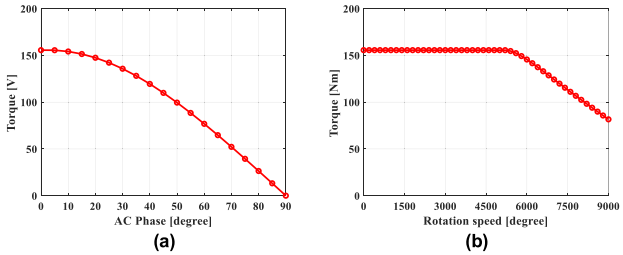

FIGURE 7. The T-β curve and T-N curve of the 3D-FEA (a) T-β curve. (b) T-N curve.

TABLE 2. Analysis results comparison of the 3D and Quasi-4.

3D-FEA	*Value*	*Unit*
Phase Back-EMF	161.11	V_{rms}
Line-to-Line Back-EMF	277.85	V_{rms}
λ_d	0.0534	H
λ_q	0.0249	H
Current	194.38	A_{pk}
Voltage	249.61	V
Average torque	155.62	Nm

IV. QUASI-3D ANALYSIS METHOD

A. PRINCIPLE OF THE QUASI-3D ANALYSIS METHOD

The Fig. 8 is a conceptual diagram of quasi-3D [18], and quasi-3D is a method of approximately calculating the results of 3D FEA by combining multiple 2D FEA results [19], [20], [21], [22], [23]. The straight-line motion analysis is performed rather than rotational motion analysis by dividing the shape of a cylinder-shaped 3D motor into N pieces and spreading the shape of the pillar in a straight-line. Therefore, the force value, not the torque value, is extracted and converted into torque through the following equation.

$$Q_r = r_i + (r_o - r_i)/Q_n \cdot (Q_i - \frac{1}{2}) \tag{19}$$

$$T = Q_r \times F \tag{20}$$

where Q_r is the distance from the center of the motor to the i^{th} quasi segment, r_i means the inner radius of the rotor of the motor, r_o means the outer radius of the rotor of the motor, Q_n means the total number of quasi segments, Q_i means the i^{th} quasi segment, and F means for the force in straight-line motion.

The (19) is equally applicable to the stator of the motor, and all it needs to do is change the parameters for the rotor to the stator parameters. If the torque is expressed as a rotational motion, it can be expressed as a product of the moment of inertia $I$and the angular acceleration α,and if expressed as a straight-line motion, it is equal to the product of the force Fon the straight-line motion and the distance from the center of the motor or radius of the motor. The similar value to the torque of the rotational motion analysis can be obtained through the force and the distance from the center of the motor of each quasi segment. In addition to torque, it has the advantage of being able to extract all data that can be extracted from 3D analysis such as torque ripple, voltage, magnetic flux-linkage, and iron loss data.

Therefore, the quasi-3D method is applied to studies that require a lot of analysis, such as analysis by shape and analysis according to design variables in the initial design of the motor, so that the analysis time can be shortened. In addition, it is judged to be sufficiently applicable in the optimal design since the trend of quasi-3D analysis does not change compared to the 3D analysis results.

B. VERIFICATION OF THE QUASI-3D ANALYSIS METHOD

The quasi-3D is applied to a propulsion motor for UAM to verify the validity. The Fig. 9 shows the results of the divided phase back-electromotive force (back-EMF) of each quasi segment and the combined phase back-EMF of quasi-N, and as described above, several analysis results are combined into one.

The quasi-3D method has several advantages, but since it is a method of approximating 3D analysis into multiple 2D analyses, the accuracy of the analysis depends on the number of segments. Therefore, it is necessary to determine the appropriate number of segments, and for this purpose the results of the analysis of phase back-EMF and line to line back-EMF according to quasi segment are summarized in Table 3. It is judged that the analysis results have been sufficiently converged when the quasi-4 segments. In this paper, the four segments are used in consideration of the accuracy of quasi-3D based on the analysis results. However, since the number of segments may vary slightly from model to model, it is necessary to find the appropriate number of segments for the model when using the quasi-3D method.

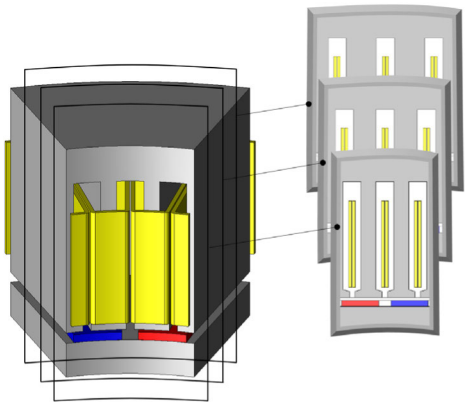

FIGURE 8. Conceptual diagram of the Quasi-3D.

The Fig. 10 shows the comparison of phase back-EMF and line to line back-EMF of quasi-4 and 3D analysis. Although some errors occur, the results are quite similar, and the waveform is the same. The Table 4 summarizes the detailed analysis results for Fig. 10. The errors at phase back-EMF and line to line back-EMF are 0.78% and 0.80%, respectively, which show an error rate within 1%. In addition, the Table 5 shows the comparison of the analysis time between the 3D analysis and the quasi-4 segment analysis result. The analysis

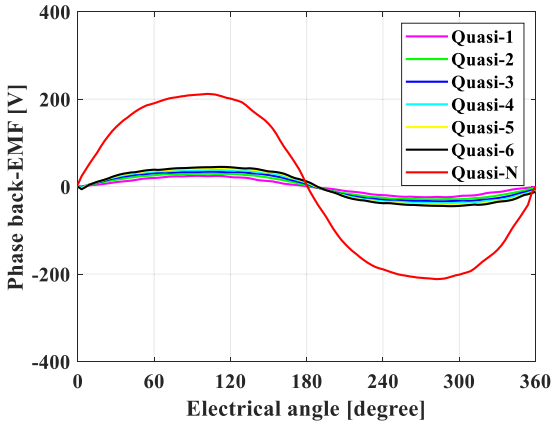

FIGURE 9. Phase Back-EMF of each Quasi segment and the sum of the Quasi segments (Quasi-N).

TABLE 3. Comparison of analysis results according to the number of quasi segments.

Model	*Phase Back-EMF*	*Line-to-Line Back-EMF*
Quasi-1	169.27 [V_{rms}]	286.69 [V_{rms}]
Quasi-2	164.07 [V_{rms}]	278.39 [V_{rms}]
Quasi-3	162.78 [V_{rms}]	276.34 [V_{rms}]
Quasi-4	162.36 [V_{rms}]	275.64 [V_{rms}]
Quasi-5	162.17 [V_{rms}]	275.30 [V_{rms}]
Quasi-6	162.08 [V_{rms}]	275.15 [V_{rms}]
Quasi-7	162.08 [V_{rms}]	275.19 [V_{rms}]
Quasi-8	162.03 [V_{rms}]	275.09 [V_{rms}]

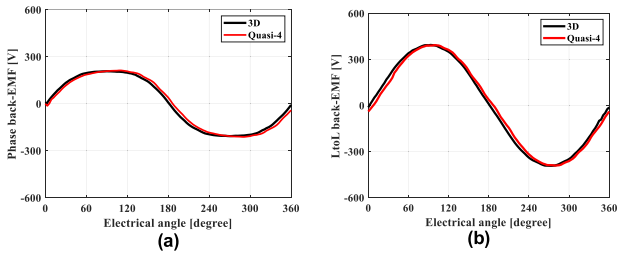

FIGURE 10. Back-EMF comparison of the Quasi-3D and 3D (a) Phase Back-EMF (b) Line to Line Back-EMF.

TABLE 4. Analysis results comparison of the 3D and Quasi-4.

Model	*3D*	*Quasi-4*	Error rate
Phase Back-EMF	161.11 [V_{rms}]	162.36 [V_{rms}]	0.78 [%]
Line-to-Line Back-EMF	277.85 [V_{rms}]	275.64 [V_{rms}]	0.80 [%]

time can be reduced by 96.0% when using the quasi-3D method. Through comparison of analysis results and analysis time, it is verified that the quasi-3D method is quite effective.

V. 3D – 1STEP ANALYSIS METHOD

A. PRINCIPLE OF THE 3D-1STEP ANALYSIS METHOD

In general, the analysis is performed when analyzing a motor by dividing the period of electrical angle by the appropriate number of analysis steps. In [27], the analysis was conducted by dividing one period of electrical angle into 120 steps, and the results are quite similar to the experimental results. Thererfore, it was determined that about 120 steps were sufficiently reliable, and this paper also divided the 3D analysis into 120 steps.

TABLE 5. Analysis time of the 3D and Quasi-4.

Model	*3D*	*Quasi-4*	Reduction rate
Analysis time	4892.89 [s]	197.32 [s]	96.0 [%]

The 3D-1step analysis method only analyzes the initial position of the rotor with the d-q axis aligned. Since the anlaysis is performed only at the initial position, the orange points in Fig. 11(a), that is the magnetic flux linkage of each phase coil can be extracted at the 0 degree of the electrical angle. If this is converted to d-q axis magnetic flux linkage using (3) and (4), as shown in Fig. 11(b), it can be seen that the average value of the magnetic flux linkage of 3D-120steps analysis and the result of 3D-1step analysis are very similar. The Table 6 shows that the error rates of the d-q axis magnetic flux linkages are quite similar, 1.12% and 0.8%, respectively.

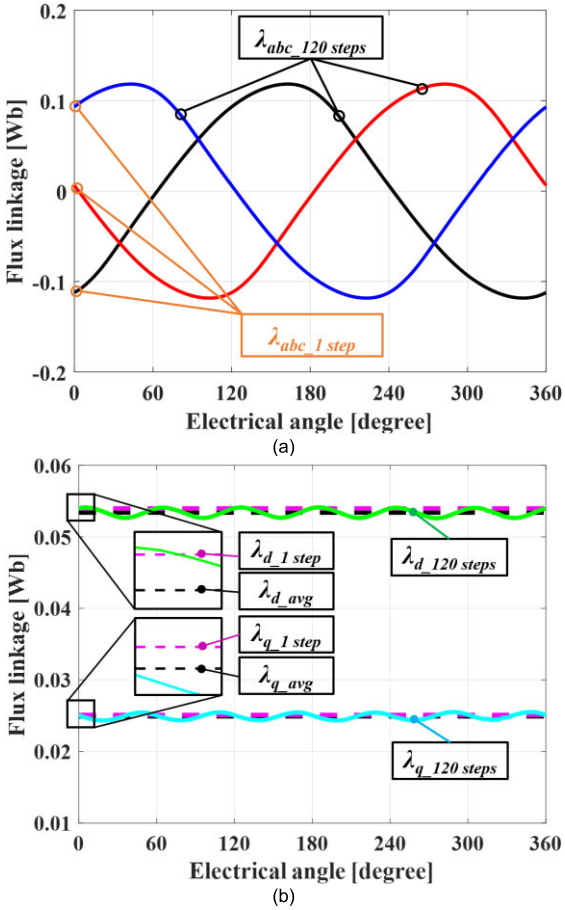

FIGURE 11. The magnetic flux linkage comparison of the 3D–120steps and 3D–1step. (a) Magnetic flux linkage of each phase coils. (b) d-q axis transformed magnetic flux linkage.

B. VERIFICATION OF THE 3D-1STEP ANALYSIS METHOD

A T-β curve and T-N curve are extracted for validation of the 3D-1step analysis method. The current phase angle

TABLE 6. Comparison of flux linkage of the 3D – 120steps and 3D – 1step.

Model	*3D - 120steps*	*3D – 1step*	Error rate
λ_d	0.0534 [H]	0.0540 [H]	1.12 [%]
λ_q	0.0249 [H]	0.0251 [H]	0.80 [%]

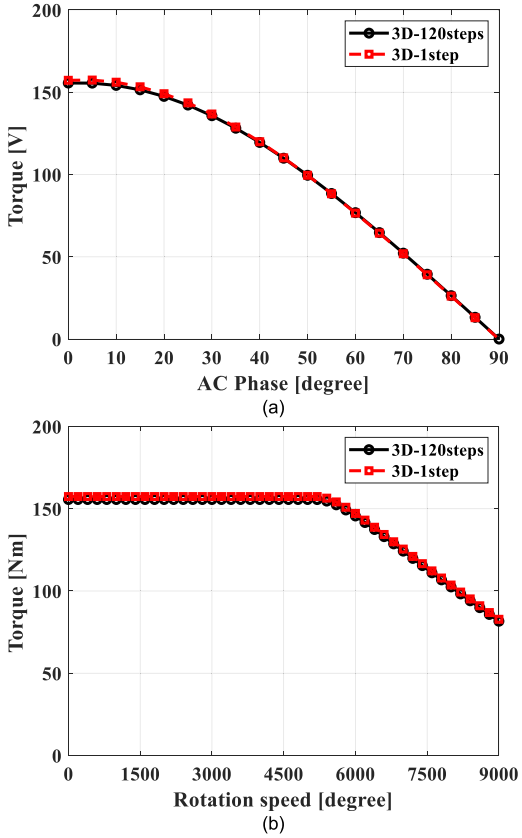

FIGURE 12. The T-β curve and T-N curve comparison of the 3D–120steps and 3D–1step. (a) T-β curve. (b) T-N curve.

TABLE 7. Analysis results of the 3D – 120steps and 3D – 1step.

Model	*3D - 120steps*	*3D – 1step*	Error rate
Average torque	155.62 [Nm]	157.28 [Nm]	1.06 [%]
Voltage	249.61 [V]	252.15 [V]	1.02 [%]

TABLE 8. Analysis time of the 3D – 120steps and 3D – 1step.

Model	*3D - 120steps*	*3D - 1step*	Reduction rate
Analysis time	167,140 [s]	13,117 [s]	92.2 [%]

TABLE 9. Analysis results of the Quasi-3D and EQAM.

Model	*Quasi-3D*	*EQAM*	Error rate
Average torque	153.72 [Nm]	155.31 [Nm]	1.03 [%]
Voltage	240.02 [V]	242.42 [V]	1.00 [%]

interpreted at intervals of 5 degrees from 0 to 90 degrees. The Fig. 12(a) represents a T-β curve of 3D-120steps and 3D-1step and Fig. 12(b) represents a T-N curve of 3D-120steps and 3D-1step, and the torque and voltage error rates for

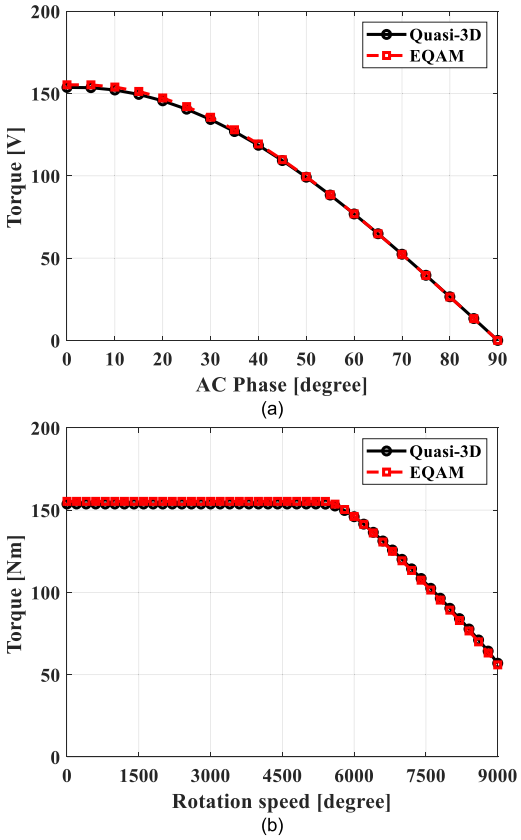

FIGURE 13. The T-β curve and T-N curve comparison of the Quasi-3D and EQAM. (a) T-β curve. (b) T-N curve.

TABLE 10. Analysis time and file capacity of the Quasi-3D and EQAM.

Model	*Quasi-3D*	*EQAM*	Reduction rate
Analysis time	5,112 [s]	1,475 [s]	71.2 [%]
File capacity	892 [MB]	24.6 [MB]	97.2 [%]

each current phase angle are quite similar within 1.5%. The torque and voltage error at the operating point are within 1.1%, and the anlaysis time is reduced by about 92% to 167,140s and 13,117s, respectively, which are summarized in Table 7 and Table 8. The excellence of the 3D-1step analysis method is confirmed that the analysis time reduction rate is significantly higher than the error rate as a result of the verification.

TABLE 11. Analysis results of the 3D – 1step and EQAM.

Model	*3D – 1step*	*EQAM*	Error rate
Average torque	157.28 [Nm]	155.31 [Nm]	1.25 [%]
Voltage	252.15 [V]	242.42 [V]	3.86 [%]

TABLE 12. Analysis time and file capacity of the 3D – 1step and EQAM.

Model	*3D – 1step*	*EQAM*	Reduction rate
Analysis time	13,117 [s]	1,475 [s]	88.8 [%]
File capacity	442 [MB]	24.6 [MB]	94.4 [%]

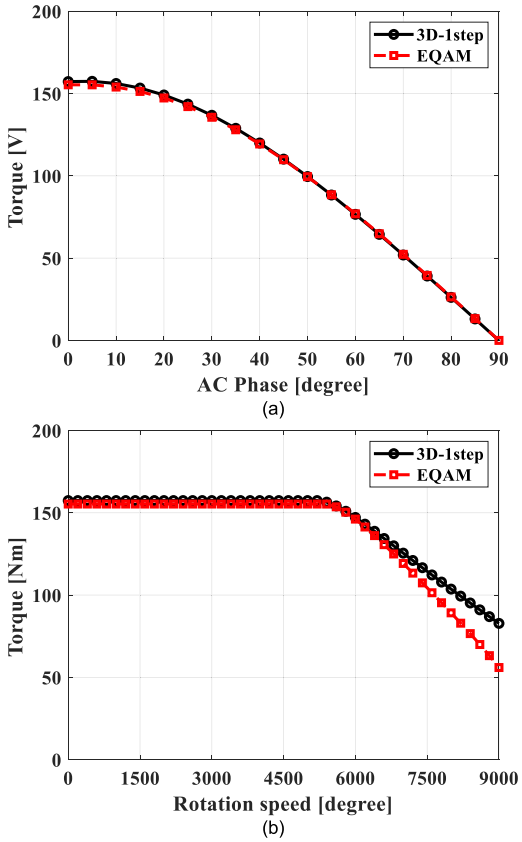

FIGURE 14. The T-β curve and T-N curve comparison of the 3D-1step and EQAM. (a) T-β curve. (b) T-N curve.

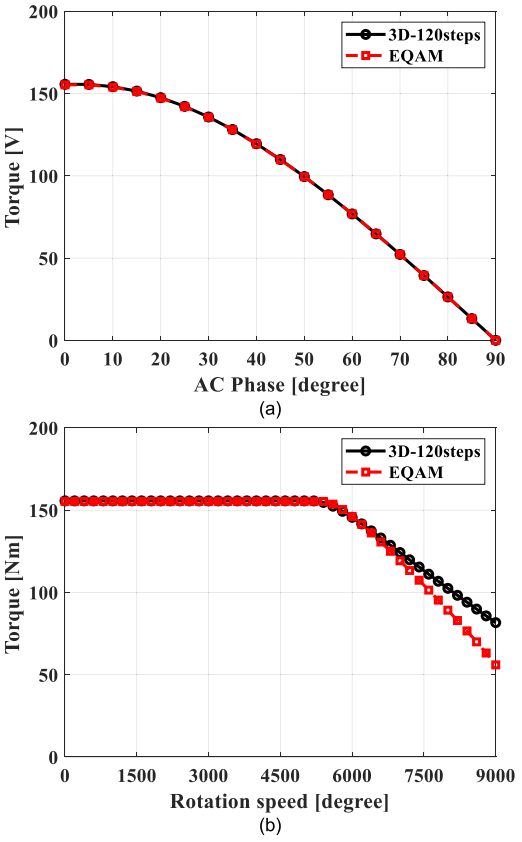

FIGURE 15. The T-β curve and T-N curve comparison of the 3D-120steps and EQAM. (a) T-β curve. (b) T-N curve.

VI. EVOLVED QUASI-3D ANALYSIS METHOD

In the case of quasi-3D analysis method, 3D analysis can be equalized to 2D analysis to reduce analysis time. However, since this method also interprets all steps, if the number of quasi segments increases for interpret accuracy, the interpretation time will increase. The 3D-1step analysis method can also significantly reduce the analysis time compared to interpreting 120 steps. However, 3D modeling is essential since this method eventually requires 3D analysis at least once. This can not be confirmed by interpretation time. However, it will be a huge burden for motor designers considering actual modeling efforts. Therefore, in this paper, the EQAM is proposed that replaces 3D analysis by interpreting only 1 step of the 2D model by applying these two methods at the same time. As a result, the interpretation time can be significantly reduced. The EQAM takes about 1/100 of the analysis time compared to the existing 3D analysis. That is, 100 analysis results can be confirmed in time to check only one 3D analysis result. Therefore, the trend of design variables for various objective functions in the early steps of motor design. Additionally, although there can be some errors between the EQAM analysis results and the existing 3D analysis results, a model with excellent electromagnetic analysis results in EQAM is also excellent in 3D analysis. In other words, the EQAM can be fully utilized in the detailed design or optimal design step since the tendency of the model does not change.

The EQAM is validated by comparing the average torque and voltage of the operating point, the analysis time and file capacity for deriving the T-β curve. The current phase angle is interpreted at intervals of 5 degrees from 0 to 90 degrees to derive the T-β curve and the T-N curve are extracted using T-β curve.

TABLE 13. Analysis results of the 3D – 120steps and EQAM.

Model	*3D - 120steps*	*EQAM*	Error rate
Average torque	155.62 [Nm]	155.31 [Nm]	0.20 [%]
Voltage	249.61 [V]	242.42 [V]	2.88 [%]

TABLE 14. Analysis time and file capacity of the 3D – 120steps and EQAM.

Model	*3D - 120steps*	*EQAM*	Reduction rate
Analysis time	167,140 [s]	1,475 [s]	99.1 [%]
File capacity	5.67 [GB]	24.6 [MB]	99.6 [%]

The Fig. 13(a) represents a T-β curve of Quasi-3D and EQAM and Fig. 13(b) represents a T-N curve of Quasi-3D and EQAM, and the torque and voltage error rates for each current phase angle are quite similar within 1.1%. The torque and voltage error at the operating point are within 1.0%,

and the analysis time is reduced by about 71% and the file capacity is reduced by 97.2, which are summarized in Table 9 and Table 10. The Fig. 14(a) represents a T-β curve of 3D-1step and EQAM and Fig. 14(b) represents a T-N curve of 3D-1step and EQAM, and the torque and voltage error rates for each current phase angle are quite similar within 1.3%. The torque and voltage error at the operating point are within 4.0%, and the analysis time is reduced by about 89% and the file capacity is reduced by 94.4%, which are summarized in Table 11 and Table 12. In the Fig. 15, the 3D-120steps analysis and the EQAM analysis results can be compared. The torque error rate according to the current phase angle is considerably similar with an average of 0.2%. However, in terms of voltage, the average error rate is 7.5%, and the error rate gradually increased at a current phase angle of 45 degrees or higher. The error rate can be increase because the voltage magnitude decreases even with the same voltage difference. However, as can be seen from the comparison of T-N curve in Fig. 15(b), the voltage of the EQAM in the field weaking area is calculated larger, causing the torque to drop more steeply in the T-N curve. This error is undoubtedly a problem to be solved in future research. However, the average torque error rate at the operating point is 0.20% and the voltage error rate is about 2.9% as shown in Table 13 and the analysis time is 99.1% and the file capacity is reduced by 99.6% as shown in Table 14. Therefore, the EQAM shows a significantly larger reduction rate than the error rate, which is sufficient to confirm its superiority.

VII. CONCLUSION

The EQAM proposed in this paper replaces 3D analysis with 1step analysis of the 2D model by applying the 3D-1step analysis method to the existing quasi-3D analysis method to maximize the reduction of analysis time for models that structurally require 3D analysis such as AFPMM. First, the possibility of the proposed method is confirmed through comparison of quasi-3D and 3D analysis, and the results of 3D analysis and EQAM analysis are compared to verify the validity of the proposed method. The operating point is satisfied with an average torque error rate of 0.20% and a voltage error rate of 2.88%, and the analysis time reduction rate of 99.1% and file capacity reduction rate of 99.6% are confirmed when deriving the T-β curve, confirming the excellence of the proposed method. Therefore, the proposed method is expected to be applied to various fields and studies that require 3D FEA, which will be of great help in solving the temporal problems faced by researchers conducting the study.

REFERENCES

[1] E. C. Pinto Neto, D. M. Baum, J. R. de Almeida, J. B. Camargo, and P. S. Cugnasca, "A trajectory evaluation platform for urban air mobility (UAM)," *IEEE Trans. Intell. Transp. Syst.*, vol. 23, no. 7, pp. 9136–9145, Jul. 2022.

[2] T. Lee, H. Lee, P. Jang, Y. Hwang, and K. Nam, "Position fault detection for UAM motor with seamless transition," *IEEE Access*, vol. 9, pp. 168042–168051, 2021.

[3] B. Hu and X. Dong, "Communications channel characteristics due to aircraft body blockage in urban air mobility," *IEEE Commun. Lett.*, vol. 27, no. 1, pp. 24–27, Jan. 2023.

[4] A. P. Cohen, S. A. Shaheen, and E. M. Farrar, "Urban air mobility: History, ecosystem, market potential, and challenges," *IEEE Trans. Intell. Transp. Syst.*, vol. 22, no. 9, pp. 6074–6087, Sep. 2021.

[5] R. Hoffmann, H. Nishimura, and R. Latini, "Urban air mobility situation awareness from enterprise architecture perspectives," *IEEE Open J. Syst. Eng.*, vol. 1, pp. 12–25, 2023.

[6] S. H. Kim, "Receding horizon scheduling of on-demand urban air mobility with heterogeneous fleet," *IEEE Trans. Aerosp. Electron. Syst.*, vol. 56, no. 4, pp. 2751–2761, Aug. 2020.

[7] S. Naga, M. Neha, and V. Vitika, "Urban air mobility (UAM) market," Allied Market Research, Wilmington, NC, USA, Tech. Rep. A06443, Sep. 2022.

[8] C. Reiche, A. P. Cohen, and C. Fernando, "An initial assessment of the potential weather barriers of urban air mobility," *IEEE Trans. Intell. Transp. Syst.*, vol. 22, no. 9, pp. 6018–6027, Sep. 2021.

[9] G. Grandl et al., "The future of vertical mobility sizing the market for passenger, inspection, and goods services until 2035," Porsche Consult., Munich, Germany, Tech. Rep. 2, 2018. Accessed: Oct. 31, 2022. [Online]. Available: https://fedotov.co/wp-content/uploads/2018/03/Future-of-Vertical-Mobility.pdf

[10] N. Hohmann, S. Brulin, J. Adamy, and M. Olhofer, "Three-dimensional urban path planning for aerial vehicles regarding many objectives," *IEEE Open J. Intell. Transp. Syst.*, vol. 4, pp. 639–652, 2023.

[11] A. Dwivedi, S. K. Singh, and R. K. Srivastava, "Analysis and performance evaluation of axial flux permanent magnet motors," *IEEE Trans. Ind. Appl.*, vol. 54, no. 2, pp. 1765–1772, Mar. 2018.

[12] B. Cheng, G. Pan, and Z. Mao, "Analytical calculation and optimization of the segmented-stator dual-rotor axial flux permanent magnet motors," *IEEE Trans. Magn.*, vol. 56, no. 11, pp. 1–9, Nov. 2020.

[13] W. Tong, S. Dai, S. Li, J. Li, and R. Tang, "Modeling and analysis of axial flux permanent magnet machines with coexistence of rotor radial deviation and angular eccentricity," *IEEE Trans. Energy Convers.*, vol. 35, no. 4, pp. 2181–2190, Dec. 2020.

[14] O. Taqavi and N. Taghavi, "Development of a mixed solution of Maxwell's equations and magnetic equivalent circuit for double-sided axial-flux permanent magnet machines," *IEEE Trans. Magn.*, vol. 57, no. 4, pp. 1–11, Apr. 2021.

[15] M. R. Zakir, J. Ikram, S. I. Shah, S. S. H. Bukhari, S. Ali, and F. Marignetti, "Performance improvement of axial flux permanent magnet machine with phase group concentrated coil winding," *Energies*, vol. 15, no. 19, p. 7337, Oct. 2022, doi: 10.3390/en15197337.

[16] Z. Mahmood, J. Ikram, R. Badar, S. S. H. Bukhari, M. A. A. Shah, A. A. Memon, and M. Huba, "Minimization of torque ripples in multi-stack slotted stator axial-flux synchronous machine by modifying magnet shape," *Mathematics*, vol. 10, no. 10, p. 1653, May 2022, doi: 10.3390/math10101653.

[17] S. Amin, S. Madanzadeh, S. Khan, S. S. H. Bukhari, F. Akhtar, and J.-S. Ro, "Effect of the magnet shape on the performance of coreless axial flux permanent magnet synchronous generator," *Electr. Eng.*, vol. 104, no. 2, pp. 959–968, Apr. 2022, doi: 10.1007/s00202-021-01338-x.

[18] B.-O. Tak and J.-S. Ro, "Analysis and design of an axial flux permanent magnet motor for in-wheel system using a novel analytical method combined with a numerical method," *IEEE Access*, vol. 8, pp. 203994–204011, 2020.

[19] Y. Du, Y. Huang, B. Guo, F. Peng, and J. Dong, "Semianalytical model of multiphase Halbach array axial flux permanent-magnet motor considering magnetic saturation," *IEEE Trans. Transport. Electrific.*, vol. 9, no. 2, pp. 2891–2901, Jun. 2023.

[20] K.-H. Kim and D.-K. Woo, "Novel quasi-three-dimensional modeling of axial flux in-wheel motor with permanent magnet skew," *IEEE Access*, vol. 10, pp. 98842–98854, 2022.

[21] B. Guo, Y. Du, Z. Djelloul-Khedda, F. Peng, J. Dong, Y. Huang, F. Dubas, and K. Boughrara, "Nonlinear semianalytical model for axial flux permanent-magnet machine," *IEEE Trans. Ind. Electron.*, vol. 69, no. 10, pp. 9804–9816, Oct. 2022.

[22] H. Zhao, K. T. Chau, T. Yang, Z. Song, and C. Liu, "A novel quasi-3D analytical model for axial flux motors considering magnetic saturation," *IEEE Trans. Energy Convers.*, vol. 37, no. 2, pp. 1358–1368, Jun. 2022.

[23] W. Tong, S. Wang, S. Dai, S. Wu, and R. Tang, "A quasi-three-dimensional magnetic equivalent circuit model of a double-sided axial flux permanent magnet machine considering local saturation," *IEEE Trans. Energy Convers.*, vol. 33, no. 4, pp. 2163–2173, Dec. 2018.
[24] D. Baimel, J. Belikov, J. M. Guerrero, and Y. Levron, "Dynamic modeling of networks, microgrids, and renewable sources in the dq0 reference frame: A survey," *IEEE Access*, vol. 5, pp. 21323–21335, 2017.
[25] X. Zhou, J. Sun, H. Li, and X. Song, "High performance three-phase PMSM open-phase fault-tolerant method based on reference frame transformation," *IEEE Trans. Ind. Electron.*, vol. 66, no. 10, pp. 7571–7580, Oct. 2019.
[26] C. J. O'Rourke, M. M. Qasim, M. R. Overlin, and J. L. Kirtley, "A geometric interpretation of reference frames and transformations: *dq*0, Clarke, and Park," *IEEE Trans. Energy Convers.*, vol. 34, no. 4, pp. 2070–2083, Dec. 2019.
[27] J.-C. Son and D.-K. Lim, "Novel method of deriving torque and speed curve of the permanent magnet synchronous motor using initial state finite element analysis," *IEEE Trans. Magn.*, vol. 58, no. 8, pp. 1–6, Aug. 2022.

JONG-MIN AHN received the M.S. degree in electrical engineering from the School of Electrical Engineering, University of Ulsan, South Korea, in 2022, where he is currently pursuing the Ph.D. degree. His research interest includes the analysis and optimal design of electrical machines.

HAN-KYEOL YEO received the B.S. degree in electronic and electrical engineering from Sungkyunkwan University, Suwon, South Korea, in 2012, and the Ph.D. degree in electrical engineering from Seoul National University, Seoul, South Korea, in 2018, through the combined master's and Ph.D. program.

From 2018 to 2021, he was a Senior Research Engineer with the Department of Advanced Electrification Engineering Design Team, Hyundai Motor Company, Hwaseong-si, South Korea. He is currently an Assistant Professor with the Division of Electrical and Electronic Engineering, The University of Suwon, Hwaseong-si. His research interest includes the analysis and optimal design of electric machines.

JI-YEON KIM received the M.S. degree in mechanical engineering from the Department of Mechanical Engineering, Hanyang University, South Korea, in 2012. She is currently developing and researching motors for driving vehicles with Hyundai Motor Company.

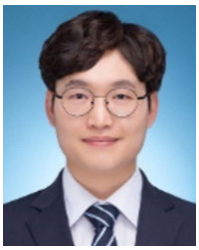

DONG-HEE LEE received the M.S. degree in automotive engineering from the Department of Vehicle Control Engineering, Hanyang University, South Korea, in 2019. He is currently developing and researching motors for driving vehicles with Hyundai Motor Company.

DONG-KUK LIM received the B.S. degree in electrical engineering from Dongguk University, Seoul, South Korea, in 2010, and the Ph.D. degree in electrical engineering from Seoul National University, Seoul, in 2017, through the combined master's and Ph.D. program.

In 2017, he was with the Electrical Power Engineering Team, Hyundai Mobis Company, South Korea, as a Senior Research Engineer. He is currently an Assistant Professor with the School of Electrical Engineering, University of Ulsan, South Korea. His research interest includes the analysis and optimal design of electrical machines.